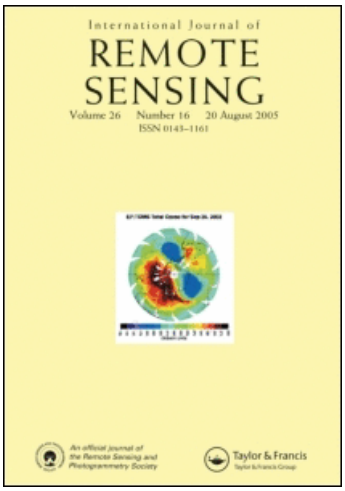

International Journal of Remote Sensing
Publication details, including instructions for authors and subscription information:
http://www.informaworld.com/smpp/title~content=t713722504

Multi-scale thermal pattern monitoring of a large lake (Lake Geneva) using a multi-sensor approach

D. Oesch [a]; J. -M. Jaquet [bc]; R. Klaus [bc]; P. Schenker [d]
[a] Syngenta International, Basel, Switzerland [b] UNEP-GRID, Geneva, Switzerland [c] UTED-S, Earth Science Section, University of Geneva, Switzerland [d] Department of Environmental Sciences, Swiss Federal Institute of Technology, Zurich, Switzerland

First Published:October2008

To cite this Article Oesch, D., Jaquet, J. -M., Klaus, R. and Schenker, P.(2008)'Multi-scale thermal pattern monitoring of a large lake (Lake Geneva) using a multi-sensor approach',International Journal of Remote Sensing,29:20,5785 — 5808
To link to this Article: DOI: 10.1080/01431160802132786
URL: http://dx.doi.org/10.1080/01431160802132786

International Journal of Remote Sensing
Vol. 29, No. 20, 20 October 2008, 5785–5808

Taylor & Francis
Taylor & Francis Group

Multi-scale thermal pattern monitoring of a large lake (Lake Geneva) using a multi-sensor approach

D. OESCH*†, J.-M. JAQUET‡§, R. KLAUS‡§ and P. SCHENKER¶
†Syngenta International, Basel, Switzerland
‡UNEP-GRID, Geneva, Switzerland
§UTED-S, Earth Science Section, University of Geneva, Switzerland
¶Department of Environmental Sciences, Swiss Federal Institute of Technology, Zurich, Switzerland

(*Received 26 November 2006; in final form 15 March 2008*)

The applicability of satellite imagery products from different sensors (AVHRR-derived multi-channel sea surface temperature (MCSST), MODIS sea surface temperature (SST) products 5-Min L2 Swath 1 km and Landsat TM band 6 thermal signature) for the comprehensive monitoring of temperature and its temporal patterns over a large lake is tested in this study. The coverage of cloud-free satellite data for Lake Geneva is reported throughout a year and, more specifically, during a 13 day period in summer 2003. In a second step, we demonstrate the feasibility of the AVHRR/MODIS imagery to discern day and night temperature patterns, by generating day and night climatologies and various spatial statistics over the 13 day period. The different day and night surface thermal patterns observed by satellite imagery could be linked to the thermal structure existing in deeper water using the concept of the diurnal decoupled layer. The forcing of the persistent patterns, two warm cores divided by a saddle-shaped cold anomaly, is explained by wind periodicity and insolation conditions. The patterns can be matched to features postulated by findings of different limnologists in the past. Other surface temperature related phenomena such as water upwelling and downwelling and the occurrence of plumes are related to meteorological and hydrological events. The lakewide average lake surface water temperature (LSWT) trends for day and night during the study period are roughly parallel. A sudden loss of stored heat can be explained by episodes of long fetch, synoptic wind (bise) that interrupted the predominant breeze regime.

1. Introduction

The monitoring of lake surface water temperatures (LSWT) is important for several applications, such as water quality management, numerical weather prediction or the modelling of physical properties. Many continental water bodies, such as Lake Geneva, contain a large volume and areal extent of water, resulting in a complex temperature structure in both vertical and horizontal dimensions (Strub and Powell 1986, Giovanoli 1990, Lemmin and D'Adamo 1996).

Horizontal thermal mapping of continental water bodies was achieved for the Great Lakes as early as the late 1960s (Lane 1970, Noble and Wilkerson 1970).

*Corresponding author. Email: david.oesch@syngenta.com

International Journal of Remote Sensing
ISSN 0143-1161 print/ISSN 1366-5901 online
http://www.tandf.co.uk/journals
DOI: 10.1080/01431160802132786

Satellite and airborne infrared imagery demonstrated their value in revealing detailed surface thermal patterns of Lakes Michigan and Ontario. Large-scale dynamic processes, as well as smaller scale phenomena, such as internal wave patterns and small eddies, could be confirmed.

The determination of lake thermal structure and circulation are fundamental for hydrodynamical studies. Establishing and testing physical lake models requires accurate knowledge of subsurface and surface temperature, as shown in several studies by Beletsky and Schwab (2001) and Strub and Powell (1987). Effects such as wind stress curl, topography and stratification at different scales have to be taken into account (Schwab and Beletsky 2003).

Lake Geneva (locally known as Lac Léman) is a large warm, monomictic lake with a total length of 70 km and a width of up to 14 km (figure 1). It can be divided into two sections: a deep, central/eastern basin (Grand Lac; maximum depth 310 m, mean depth 160 m, mean width 10 km) and the small and narrow Petit Lac in the west (maximum depth 70 m, mean width 4.5 km). The surrounding topography influences local winds (Lemmin *et al.* 2005). Within less than 2 km from eastern and southeastern shores, elevations of more than 1000 m above lake level can be found; the eastern part, therefore, is sheltered from most synoptic winds such as bise and vent (Bouet 1985, Wanner and Furger 1990). The central and western parts lie in a 50 km wide valley formed by the separation of the Prealps and Jura mountain ranges. Hence, episodical events of strong winds from the southwest and northeast

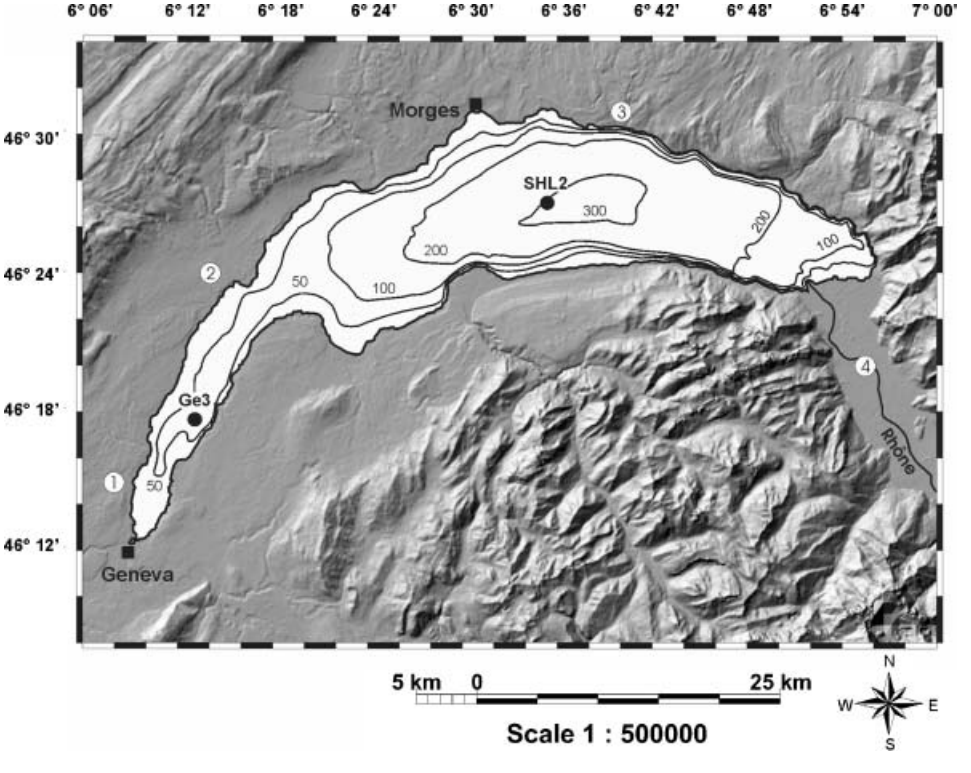

Figure 1. Topographic and bathymetric map of Lake Geneva (Lac Léman), with position of meteorological stations: 1: Geneva Airport; 2: Nyon-Changins; 3: Pully; 4: Aigle. CUEPE station is in Geneva. Ge3 and SHL2 are sampling points. Isodepths are in metres.

dominate in the western part of the lake, and may last from several hours to several days. Lemmin and D'Adamo (1996) observed that the strong winds from northeast cause thermocline depressions of more than 20 m in the western part. A persistent cyclonic circulation in the central part of the lake could be related to cyclonic vorticity in the diurnal wind pattern, in accordance with a direct circulation mechanism proposed by Strub and Powell (1986). Recent analysis of currents and thermocline depth oscillations by Lemmin *et al.* (2005) have been identified as whole basin internal standing wave (seiches) modes excited by wind action, contrary to the earlier findings by Bohle-Carbonell (1991), who suggested that basin-wide modes did not exist.

For Lake Geneva, the thermal structure is well known in the vertical dimension, at a monthly or bi-weekly temporal frequency for the last 20 years at two monitoring stations in the Petit Lac (Ge3) and the Grand Lac (SHL2), as shown in figure 1 (CIPEL 2005). However, the horizontal dimension is neglected and the temporal resolution of 2 weeks is low. Space-borne infrared imaging sensor systems, such as the medium resolution (1100×1100 m) advanced very high resolution radiometer (AVHRR) or moderate resolution imaging spectroradiometer (MODIS) and high resolution (30×30 m) Landsat TM could fill in the gap in spatial information. In addition, the current orbital configuration of the different medium resolution platforms results in a temporal coverage of up to 10 images within 24 h.

We have applied a methodology originally developed for marine environments on the grounds that the absorption of longwave radiation by water vapour content is taken into account by chosen split-window algorithms. The feasibility of the AVHRR sea surface temperature (SST) algorithms for the determination of continental water body surface temperature has been demonstrated for the Great Lakes (Schwab *et al.* 1992, 1999, Li *et al.* 2001) and the Canadian Lakes (Bussières *et al.* 2001), as well as in Africa (Wooster *et al.* 2001) and Continental Europe (Thiemann and Schiller 2003, Oesch *et al.* 2005).

In a previous extensive validation study for Lake Geneva by Oesch *et al.* (2005), it could be shown that the relationship between bulk temperature and LSWT strongly depends on meteorological conditions such as solar insolation and wind stress. The inter-platform comparison revealed an absolute positive bias of 0.18 K and an absolute standard deviation of 0.73 K for the AVHRR and 0.65 K and 0.92 K for the MODIS, respectively. These previous findings justify the use of AVHRR and MODIS data for the analysis of surface temperature patterns.

The purpose of this paper is to investigate both the availability and applicability of medium resolution day and night imagery for detailed thermal mapping of large to medium water bodies, such as Lake Geneva. The LSWT maps can be useful for understanding hydrological processes, such as wind related upwelling events (Mortimer 1952, Monismith 1985, 1986, Imberger and Patterson 1990) and surface water transport patterns (Strub and Powell 1986, 1987). Furthermore, such data could be implemented in near real time for the assimilation into numerical weather prediction and for LSWT climatology. A review of the relevant LSWT/SST literature and a complete discussion of the AVHRR and MODIS processing scheme used in this study can be found in Oesch *et al.* (2005).

After an inventory of available imagery from the AVHRR during the year 2003 in a mid-latitude context, we will focus our demonstration on a 12 day period of cloud-free AVHRR and MODIS imagery collected from 31 July to 12 August (totalling 105 day and night data sets. The influence of clouds, sun glint and viewing geometry

leading to signal contamination by land pixels will be investigated. We will then examine the day and night LSWT maps in terms of their horizontal variability, thereby testing for the existence of non-random, predominant patterns. Finally, the observed patterns will be explained by the physical forcing related to the geomorphological, meteorological and hydrological context.

2. Data and aggregation methods

2.1 *AVHRR-LSWT products*

AVHRR data were ingested at full resolution as a high rate picture transmission (HRPT) data stream at the University of Bern, and LSWT product generation was carried out using a comprehensive processing scheme as described by Oesch *et al.* (2005). In short, the imagery was radiometrically corrected and calibrated in physical units at full instrument resolution as acquired. The LSWT retrieval method used is based on the multi-channel sea surface temperature (MCSST) algorithm as proposed by Walton *et al.* (1998). Pixels with a scan angle greater than 50° were discarded. An orthorectification of the imagery is essential in the alpine region to overcome the displacement errors introduced by the rugged topography. Several sources of errors were corrected: cloudy pixels were flagged using CASPR (Key 2002), and imagery geocoded with sub-pixel accuracy before the subset of Lake Geneva was extracted. Since sun glint interferes with the cloud masking scheme, pixels possibly affected by specular reflection were flagged using the method proposed by Cox and Munk (1954). A land mask, based on the global self-consistent hierarchical high resolution shoreline database (GSHHS; Wessel and Smith-Walter 1996), was applied to remove land contaminated pixels. The age of the MCSST coefficients of the non-operational sensors, such as N12–N15 does introduce some errors; however, the relative temperature pattern of the lake is only affected by sensor noise (noise equivalent temperature difference at 300 K is 0.12 K according to Goodrum *et al.* (2000)).

2.2 *MODIS-LSWT products*

We used MODIS/Terra (SST) products 5-Min L2 Swath 1 km (MOD28L2) and MODIS/Aqua sea surface temperature products 5-Min L2 Swath 1 km (MYD28L2) in their third validated release (Collection 4), provided by the NASA/Goddard Earth Sciences Distributed Active Archive Center (GES DAAC; http://daac.gsfc.nasa.gov/). The 1×1 km MODIS SST products, described in Minnett *et al.* (2002), were subset and resampled to have the same dimensions as the AVHRR data sets (pixel size of 0.007° in longitude and 0.01° in latitude; Oesch *et al.* 2005). In this study, we used quality flag 2 data ('probably cloudy'), since the MODIS processing scheme in near-shore and water upwelling areas results in a relatively small amount of flag 0 (good) data, as described at http://modis-ocean.gsfc.nasa.gov/qa/terra/knownprobs/knownprobs.V3.html.

2.3 *Landsat TM-LSWTI products*

To capitalise on the advantage of high resolution Landsat data, the lake surface water temperature index (LSWTI) maps were compared with the AVHRR and MODIS LSWT maps. The LSWTI is equivalent to TM band 6 digital numbers (DNs) and is not atmospherically corrected (see table 3 below). It can be used for the

analysis of high resolution relative temperature patterns within a specific Landsat imagery, since the water vapour content of the atmosphere over Lake Geneva does not vary significantly.

2.4 *Generation of LSWT maps, statistics, climatologies and anomaly maps*

On both AVHRR and MODIS images, an additional manual cloud screening was carried out to remove water pixels contaminated by cloud edges and shadows. To allow a sensor inter-comparison between the medium resolution AVHRR/MODIS and Landsat, a second shoreline (based on the Landsat imagery) was applied to account for the higher spatial resolution of the LSWTI products. In spite of these masking operations, isolated, anomalously cold or warm pixels remained at some locations near the shoreline of the lake. Emerging from the resampling process were land-contaminated pixels acquired at higher scan angles; these were manually removed after a careful examination by the authors.

The 106 data sets were first labelled as nocturnal or diurnal images. The time at which the 106 instantaneous LSWT maps [TS] from AVHRR or MODIS were collected is shown in the graph of figure 2. The N and D labels on top indicate the successive 23 night and day subdivisions, respectively (e.g. N31 means the night between 31 July and 1 August; D1 means 1 August; N1-2 means the night between 1 and 2 August). These subdivisions are of varying length because of the variable number of collected images (from 1 to 6). Subdivisions having an acceptable number of images (>3) well spread out across night and day are underlined in figure 2, so that representative averages (climatologies) can be computed. The others (not underlined) yield either overestimated (OV) or underestimated (UN) climatologies. The horizontal axis represents the image number (1 to 106) and the vertical one is

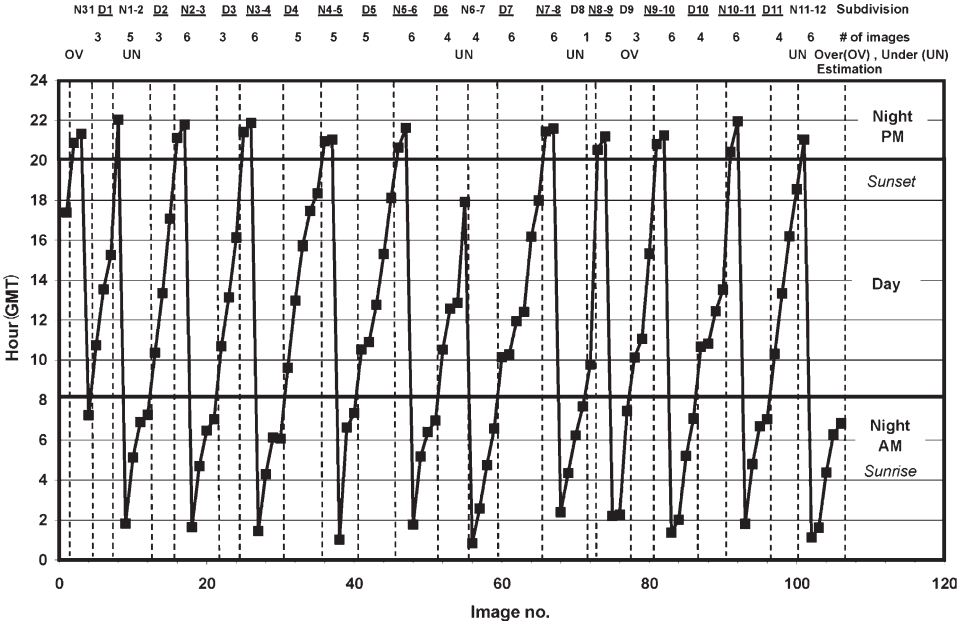

Figure 2. Acquisition time of AVHRR and MODIS images between 31 July and 12 August 2003, with number of images used.

subdivided into (from bottom to top): second part of the night (AM: 0–8 h GMT), day (8–20 h GMT) and first part of the night (PM: 20–24 h GMT).

The data on lakewide LSWT averages for various parts of the night (see table 1) were used to derive the following linear statistical relationships:

$$\mathrm{Tm}^{\mathrm{n}}_j = 0.8263\ \mathrm{Tm}^{\mathrm{PM}}_j + 3.948 \quad \left(R^2 = 0.985\right), \tag{1}$$

$$\mathrm{Tm}^{\mathrm{n}}_j = 1.0772\ \mathrm{Tm}^{\mathrm{AM}}_j - 1.7296 \quad \left(R^2 = 0.990\right) \tag{2}$$

and

$$\mathrm{Tm}^{\mathrm{n}}_j = 1.0581\ \mathrm{Tm}^{2}_j - 1.0925 \quad \left(R^2 = 0.915\right), \tag{3}$$

where j represents night (j=1,12) or day (j=1,11) interval, $\mathrm{Tm}^{\mathrm{PM}}{}_j$ is the lakewide nocturnal LSWT average computed between 8 and 12 h GMT, $\mathrm{Tm}^{\mathrm{AM}}{}_j$ is the lakewide nocturnal LSWT average computed between 0 and 8 h GMT, $\mathrm{Tm}^{2}{}_j$ is the lakewide LSWT average computed at, or close to 2 h GMT, $\mathrm{Tm}^{\mathrm{n}}{}_j$ is the lakewide nocturnal LSWT average and $\mathrm{Tm}^{\mathrm{n}}{}_j - \mathrm{Tm}^{\mathrm{PM}}{}_j$ is the difference between whole night and PM LSWT estimates.

These relationships were used to correct lakewide nocturnal LSWT average estimates ($\mathrm{Tm}^{\mathrm{n}}{}_j$) when the images were not sufficient in number, or missing in some parts of the night (see table 2 for results).

The stream of treatments applied to the AVHRR and MODIS images comprises the following steps:

Step A. For the period between 31 July and 12 August, 106 instantaneous LSWT maps $[\mathrm{TS}]_{\mathrm{i}}$ from the AVHRR or the MODIS were collected and labelled 'night' (20–8 h GMT or 21–9 h local time) and 'day' (8–20 h GMT or 9–21 h local time). See figures 4 and 5 below.

Step B. For each night (j=1,12) or day (j=1,11) interval and from a variable number of $[\mathrm{TS}]_{\mathrm{i}}$ images, computation of daily nocturnal/diurnal LSWT climatology and variability maps ($[\mathrm{mTS_n}]_j$, $[\mathrm{sTS_n}]_j$; $[\mathrm{mTS_d}]_j$, $[\mathrm{sTS_d}]_j$). Variability is expressed as standard deviation. The representativity of most of these climatology maps is considered to be good, as demonstrated below in §3.

Step C. For each night (j=1,12) or day (j=1,11) interval and from the daily nocturnal/diurnal LSWT climatology maps ($[\mathrm{mTS_n}]_{\mathrm{j}}$, $[\mathrm{mTS_d}]_{\mathrm{j}}$), computation of

Table 1. Lakewide LSWT averages (°C) for various parts of the night on each date.

Night	Tm^{n}	$\mathrm{Tm}^{\mathrm{AM}}$	Tm^{2}	$\mathrm{Tm}^{\mathrm{PM}}$	$\mathrm{Tm}^{\mathrm{n}} - \mathrm{Tm}^{\mathrm{PM}}$
31 July–1 August	22.41			22.55	−0.14
1–2 August	22.23	22.30	22.20	21.85	
2–3 August	23.45	23.30	23.00	23.81	−0.36
3–4 August	24.47	24.30	24.60	24.80	−0.33
4–5 August	25.55	25.30	24.60	25.86	−0.31
5–6 August	25.02	24.70	24.50	25.60	−0.58
6–7 August	24.30	24.30	24.00		
7–8 August	24.27	24.20	24.10	24.48	−0.21
8–9 August	24.24	24.00	24.00	24.68	−0.44
9–10 August	24.72	24.60	24.40	25.20	−0.48
10–11 August	25.35	25.10	24.90	25.92	−0.57
11–12 August	25.40	25.30	25.30	25.98	−0.58
Mean	**24.5**	**24.3**	**24.1**	**24.8**	**−0.4**

Table 2. Subdivisions devoid of a sufficient number of images to compute representative lakewide nocturnal and diurnal lake surface water temperature averages (°C). Corrected values from statistical relations (1) to (3).

Subdivision	Symptom	Tm^{PM}	Tm^{AM}	Tm^2	Tm^n or Tm^d	Tm^n corrected	Tm^d corrected	Tm^2 corrected
Night 31 July–1 August	Only 1 AM image. **Overestimation**	22.55			22.41	22.25		
Night 1–2 August	Only 1 late PM image. **Underestimation**		22.30		22.23	22.50		
Night 2–3 August	Tm^2 is not minimum.	24.80	24.30	24.60	24.47			24.0
Night 6–7 August	Lack of PM images. **Underestimation**		24.30		24.30	24.50		
Day 8 August	Only 1 image 10 AM. **Underestimation**				25.75		26.00	
Day 9 August	Lack of late afternoon image. **Slight overestimation**				27.00		26.80	
Night 11–22 August	Lack of image at 22 PM.	25.98	25.30		25.40	25.50		

nocturnal/diurnal lakewide LSWT average and standard deviation values Tm^n_j, Ts^n_j; Tm^d_j and Ts^d_j. They represent the mean LSWT of the water body and its geographical variability (see figure 7 below). On the same basis, computation of Moran's Im^n_j and Im^d_j lag-one autocorrelation coefficient, using the Idrisi AutoCorr module (Rook's case option). For an explanation of this coefficient, see http://www.geoda.uiuc.edu/support/help/glossary.html#sa and Goodchild (1988).

Step D. For each night (j=1,12) or day (j=1,11) interval and from the mean temperature map ($[mTS_n]_j$ or $[mTS_d]_j$) divided by lakewide average Tm^n_j and Tm^d_j, computation of daily nocturnal/diurnal anomaly maps ($[aTS_n]_j$, $[aTS_d]_j$). Values <1 indicate a temperature below the lakewide average, equivalent to the negative anomalies seen by Strub and Powell (1987); values >1 indicate an above lakewide average. Anomaly maps have been filtered by a mean 3×3 kernel (see figure 7 below).

Step E. For the whole period and from, respectively, 12 night and 11 day climatology maps ($[mTS_n]_j$, $[mTS_d]_j$), computation of global or quasi-decadal LSWT climatology and variability maps ($[gmTS_n]$, $[gsTS_n]$; $[gmTS_d]$, $[gsTS_d]$), with the latter expressing the variability of temperature patterns during the period.

Global climatologies were computed from daily climatologies and not from instantaneous temperature maps to compensate for the variable number of images in night or day intervals.

For the whole period and from the quasi-decadal nocturnal/diurnal LSWT climatology maps ($[gmTS_n]$, $[gmTS_d]$), computation of quasi-decadal nocturnal/diurnal lakewide LSWT average and standard deviation values (Tm^n_q, Ts^n_q; Tm^d_q, Ts^d_q). They represent the mean LSWT of the water body and its geographical variability over the whole period.

Step F. For the whole period and from quasi-decadal LSWT climatology maps ($[gmTS_n]$, $[gmTS_d]$) divided by quasi-decadal nocturnal/diurnal lakewide LSWT

average values (Tm^n_q, Tm^d_q), computation of global or quasi-decadal nocturnal and diurnal anomaly maps ([gaTSn], [gaTSd], see figures 8(*a*) and 8(*c*) below. Anomaly maps have been filtered by a mean 3×3 kernel. They are equivalent to [$gmTS_n$] and [$gmTS_d$], but with a better rendering of patterns.

Figure 3 shows the schematics of various LSWT map types and statistics.

2.5 *Meteorological observations*

Meteorological data (hourly averages of shortwave net radiation, wind force and direction, as well as rain) are available at the automated meteorological stations (ANETZ) run by MeteoSwiss at Geneva (1 in figure 1; 420 m a.s.l.), Changins (2; 430 m a.s.l.), Pully (3; 381 m a.s.l.), and Aigle (4 in figure 1; 381 m a.s.l.). Additionally, air temperature and radiation are measured in downtown Geneva by the Centre Universitaire d'Etude des Problèmes de l'Energie (CUEPE in figure 1; 430 m a.s.l.).

3. Results

3.1 *Thermal index sensitivity*

The overall performance of the lake surface temperature retrieval methods related to the different sensors is shown in table 3. For the NOAA operated satellites, NOAA 16 MCSST night passes give the best results (0.18 K bias and 0.73 K standard deviation). For the MODIS products, best results were found for the Terra

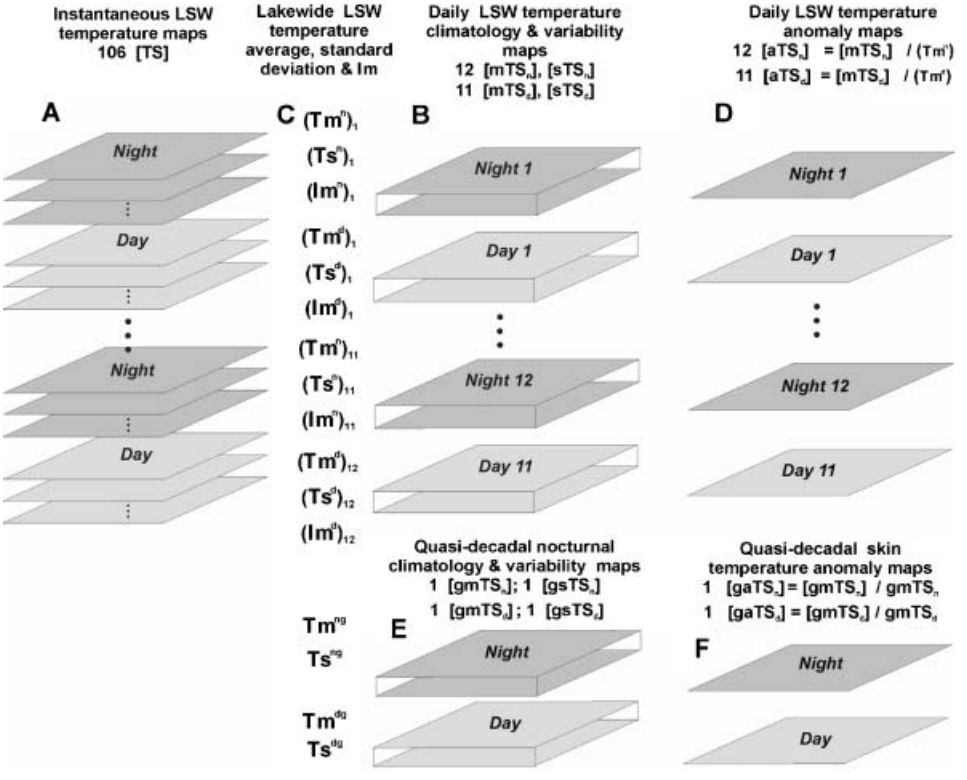

Figure 3. Schematics of various LSWT map types and statistics.

Table 3. Overall performance of the different lake surface temperature retrieval methods related to the different sensors.

SST algorithm	Bias range	Standard deviation range
NOAA–AVHRR MCSST	−0.28 to 1.5 K	0.9 to 1.6 K
MODIS SST	−1.73 to 1.9 K	0.9 to 16 K
	Temperature increment (K) per DN	
Landsat 5 TM6	0.46	

nighttime data (−0.08 K bias and 0.92 K standard deviation). A detailed discussion can be found in Oesch *et al.* (2005). For Landsat 5-derived LSWT, 1 DN represents approximately 0.5 K, as computed from Barsi *et al.* (2003) and Faour *et al.* (2004).

3.2 *Availability of thermal AVHRR imagery*

One objective of this paper is to evaluate the availability of space-borne retrieved LSWT maps for Lake Geneva in order to overcome the limited spatial coverage of in situ measurements.

In the year 2003, a total of 1536 satellite passes (AVHRR N-12, 14, 15, 16 and 17) were available for Lake Geneva. For each of them, we computed the cover fraction (%) given by the ratio of available pixels to the total number of lake pixels (931). Variations in cover fraction are related to cloudiness. Low coverage fraction phases of up to 10 days can be related to periods of cloudy weather conditions. The number of scenes includes all images with at least one pixel covering Lake Geneva. The lower occurrence of available scenes during wintertime is obviously explained by the higher frequency of clouds during this season. Although the mean monthly coverage does not exceed 63%, there is at least one image per month for which the cover is at least 80%. For applications such as continuous LSWT monitoring, each data set, consisting of up to 913 pixels with a size of $0.007^\circ \times 0.01^\circ$, compared to punctual in situ measurements, will obviously reveal new spatial information on the state of the lake. Overall, 669 800 LSWT pixels were acquired during 1586 satellite passes during 2003, compared to monthly or bi-weekly in situ measurements at Ge3 and SHL2 stations (figure 1). As mentioned above, the LSWT depends on the radiation and wind speed of the preceding days. Therefore, in situ data taken once or twice a month do not truly represent the monthly mean temperature. In addition to the available temperature profiles, LSWT can be added as spatial information by the use of satellite imagery.

For the selected period from 31 July to 12 August 2003, a combined total of up to 10 AVHRR- and MODIS-derived maps per 24 h were available. This temporal resolution, combined with the spatial resolution during cloud-free periods, permits an in-depth analysis of the surface thermal pattern evolution.

3.3 *Quality analysis of operational AVHRR/MODIS LSWT products*

Among the set of 150 images available for the mostly cloud-free study period (31 July to 12 August 2003), we have selected 12 of them to illustrate possible defaults and limitations of the imagery that would lower its quality. This typology is illustrated in figure 4. While LSWT product number 1 represents an optimal image, we find a rim of pixels missing on the north shore for the number 2 MODIS image. A large scan angle introduces a duplication of pixels in the georeferencing process,

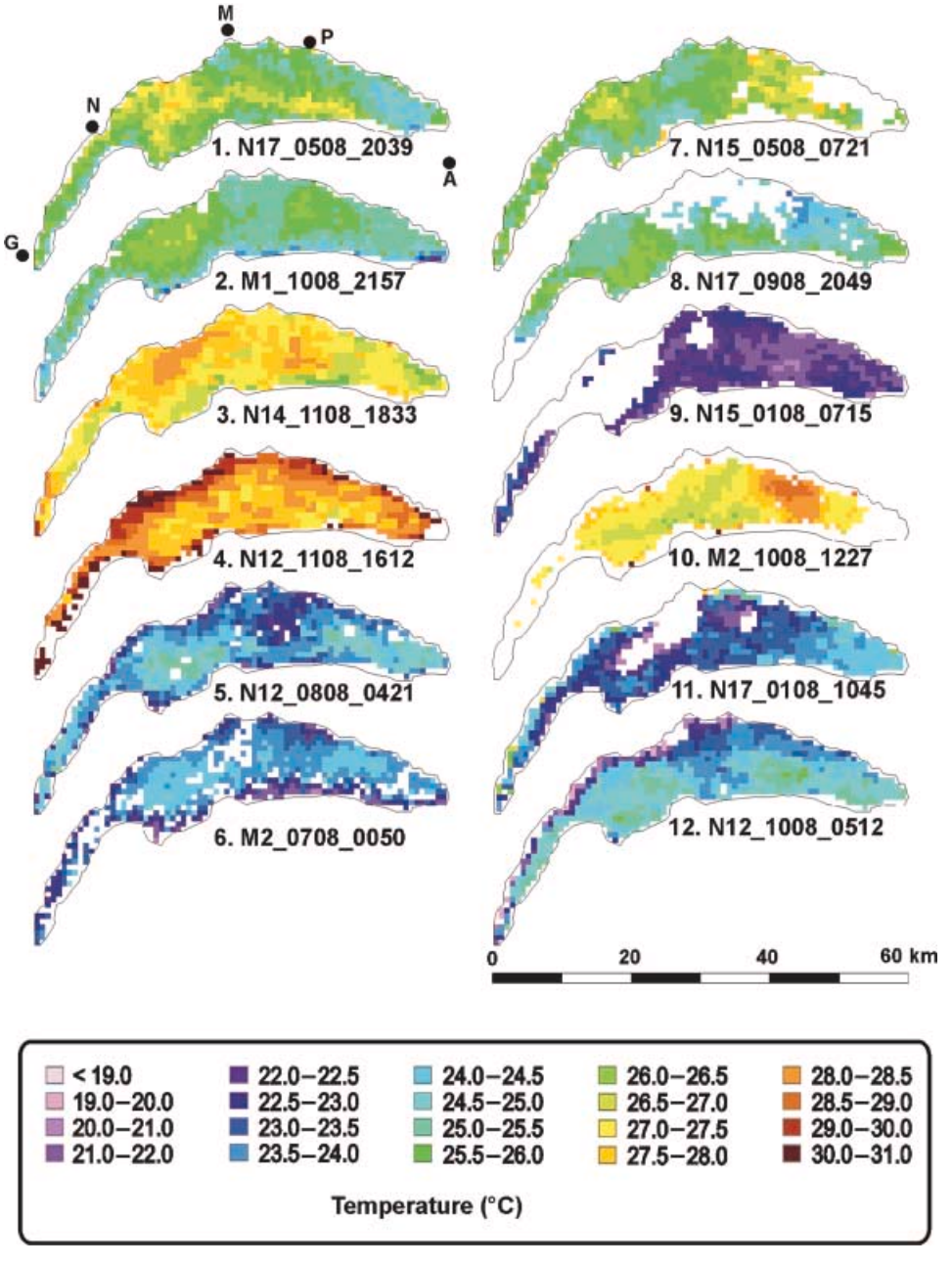

Figure 4. Quality analysis of operational AVHRR/MODIS LSWT products for Lake Geneva. Acquisition dates are given as N(AVHRR)/M(MODIS)<Satellite>_<day><month>_<hour><minute>. G: Geneva; N: Nyon-Changins; M: Morges; P: Pully; A: Aigle.

as can be identified by homogeneous horizontal stripes in cases number 3 and 4. Randomly scattered missing pixels (cases 5 and 6) are introduced by sub-pixel clouds or a stringent quality threshold scheme in the processing chain. In cases 7 to 9, large clouds obscure a significant part of the lake. Features often observed for the

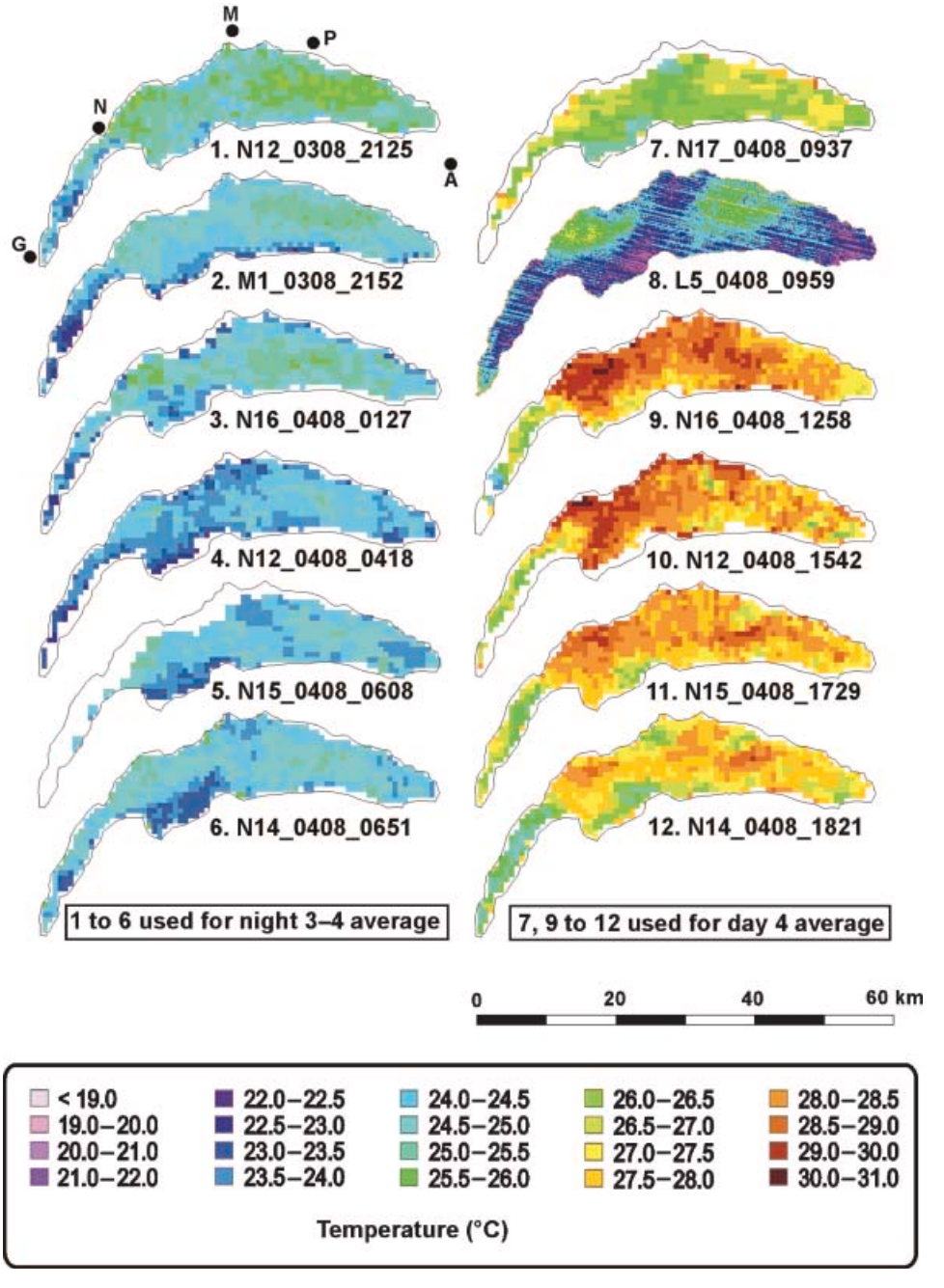

Figure 5. Interdiurnal evolution of the LSW temperature pattern on 3–4 August 2003 in Lake Geneva. Acquisition dates given as in figure 2. LSWT maps 1 to 6 represent nocturnal AVHRR/MODIS data sets, whereas maps 7 and 9 to 12 (diurnal) are significantly warmer because of solar insolation under a weak wind situation. The warm cores visible in LSWT map 7 at 0937 UTC right off Changins and off Pully are depicted in greater detail on the 60 m resolution Landsat-5 TM6 taken 21 minutes later. G: Geneva; N: Nyon-Changins; M: Morges; P: Pully; A: Aigle.

MODIS LSWT products are the missing nearshore pixels, as shown in case 10. Cloud edge/shadows not fully recognized by the operational AVHRR processing scheme are shown in cases 11 and 12, where cold-water surfaces cover the outlines of the cloud masks.

For this study, we have defined quality in terms of possibility to perform: (a) a visual identification of LSWT patterns in totality or in parts of the lake, (b) a computation of spatial statistics representative of the whole lake and (c) a manual edition of pixels. This last operation serves to remove pixels acquired at large scan angles below 50°, or those clearly contaminated by sub-pixel clouds or cloud-induced shadows (cases 4, 5, 6, 10, 11 and 12). Whereas pattern identification is nearly always possible (only partly for cases 7–12) at least in parts of the lake, computation of spatial statistics is sensitive to the areal distribution of missing pixels: if it is random and scattered (as in case numbers 5 and 6 in figure 4), it is conceivable to compute representative values of LSWT mean or standard deviation, but not Moran's Im coefficient. If sizeable parts of the lake are covered by clouds (cases 7–9), they may obliterate a high or low LSWT area present in preceding and following images, thereby inducing a bias in the lakewide statistics. These should not be computed in this case.

Out of the 150 images available for the July to August study period, after manual editing performed on 54 images (36%), 125 (83%) have been used for pattern identification and 106 (67%) for spatial statistics computations.

3.4 *Daily evolution of LSWT patterns*

Day and night instantaneous LSWT maps from 3–4 August are presented in figure 5. They have been, when necessary, manually edited following the procedure mentioned above, but not filtered. Although non-random patterns are clearly visible on these maps, some noise remains. LSWT maps 1–6 in figure 5 represent night AVHRR/MODIS data sets whereas diurnal (maps 7 and 9–12) are significantly warmer due to solar heating under a weak wind situation. As described in Oesch *et al.* (2005) for Lake Geneva and recently by Notarstefano *et al.* (2006), reduced mixing of the surface layer with the water body underneath occurred due to a lack of wind stress, resulting in a warming of several degrees of the decoupled surface layer. To confirm the existence of the temperature patterns observed by the spatial medium resolution AVHRR and MODIS sensors, we added the high resolution LSWTI map derived from Landsat TM (map 8 in figure 5). The somewhat jagged warm cores visible in the LSWT map 7 at 0937 UTC right off Nyon-Changins and off Pully are more clearly depicted on the 60 m resolution Landsat TM6 imagery taken 21 minutes later. Moreover, the four cold patches visible on the TM6 imagery are not as well resolved by the AVHRR/MODIS, and the east–west thermal trend in Petit Lac does not appear in the lower resolution image. Other examples taken from our archives (1988–2004; not shown), confirm the complementarity between these two sources of thermal information for daytime situations.

3.5 *Validation of climatologies*

The evolution of lakewide LSWT average (Tm^n and Tm^d) computed from the 106 temperature maps is plotted in figure 6, together with the lakewide average at, or close to 2 AM GMT (Tm^2). Before computing diurnal and nocturnal climatologies, we have examined to what extent the available images represent unbiased samples

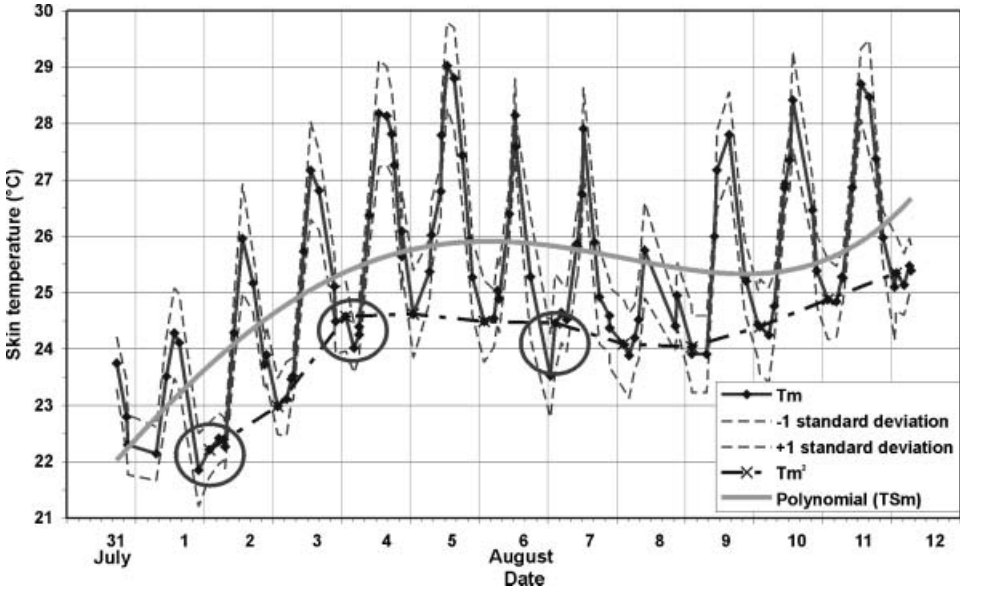

Figure 6. Evolution of lakewide instantaneous LSWT (Tm) with ± 1 standard deviation. The trend of lakeside LSWT instantaneous averages at or close to 2 h GMT (Tm^2) is shown as a dashed-dotted line. Circles show instances where Tm^2 is clearly *above* the minimal nocturnal value. The adjusted fourth-degree polynomial trend for TSm is in grey.

for the intervals (days and nights). The time frequency for the images acquisition over Lake Geneva is shown in figure 2. Out of the 23 intervals, 6 are problematic to various extents because of a lack of images in certain parts of day or night, or because Tm^2 does not represent the minimal value (tables 1 and 2). This induces either overestimation or underestimation of Tm^n and Tm^d, as shown in figure 9(*c*) below for nights N31-01, N01-02, N03-04, N06-07, day D08, D09 and night N11-12 'problematic' episodes. A statistical analysis has revealed significant correlations between the various expressions of lakewide LSWT averages. In particular, it is possible to express the whole night Tm^n as various offsets of Tm^{AM} (0–8 h), Tm^{PM} (20–24 h) and, to a lesser extent, Tm^2 (equations (1)–(3)). This makes possible a correction of averages for the problematic episodes, as shown by the empty symbols in figure 9(*b*) below. These corrections are minor ones, and do not affect the general trend of Tm^n and Tm^d over time. Hence, for the period considered, the available imagery allows the computation of representative lakewide LSWT averages and climatology maps.

3.6 *LSWT climatology mapping*

To enhance the visibility of thermal patterns, we present, in figure 7, the nocturnal and diurnal LSWT anomaly maps ($[aTS_n]$, $[aTS_d]$), computed from night and day averages (climatologies) between 31 July and 11 August 2003. The lakewide LSWT averages (Tm^n, Tm^d, Ts^n and Ts^d) and Moran's first lag autocorrelation coefficient (Im^n, Im^d) were computed from the climatologies. Wind conditions at four meteorological stations are also plotted as wind roses.

The existence of non-random thermal patterns is obvious both from visual examination of figure 7 and from the high values of Im. This coefficient is, on

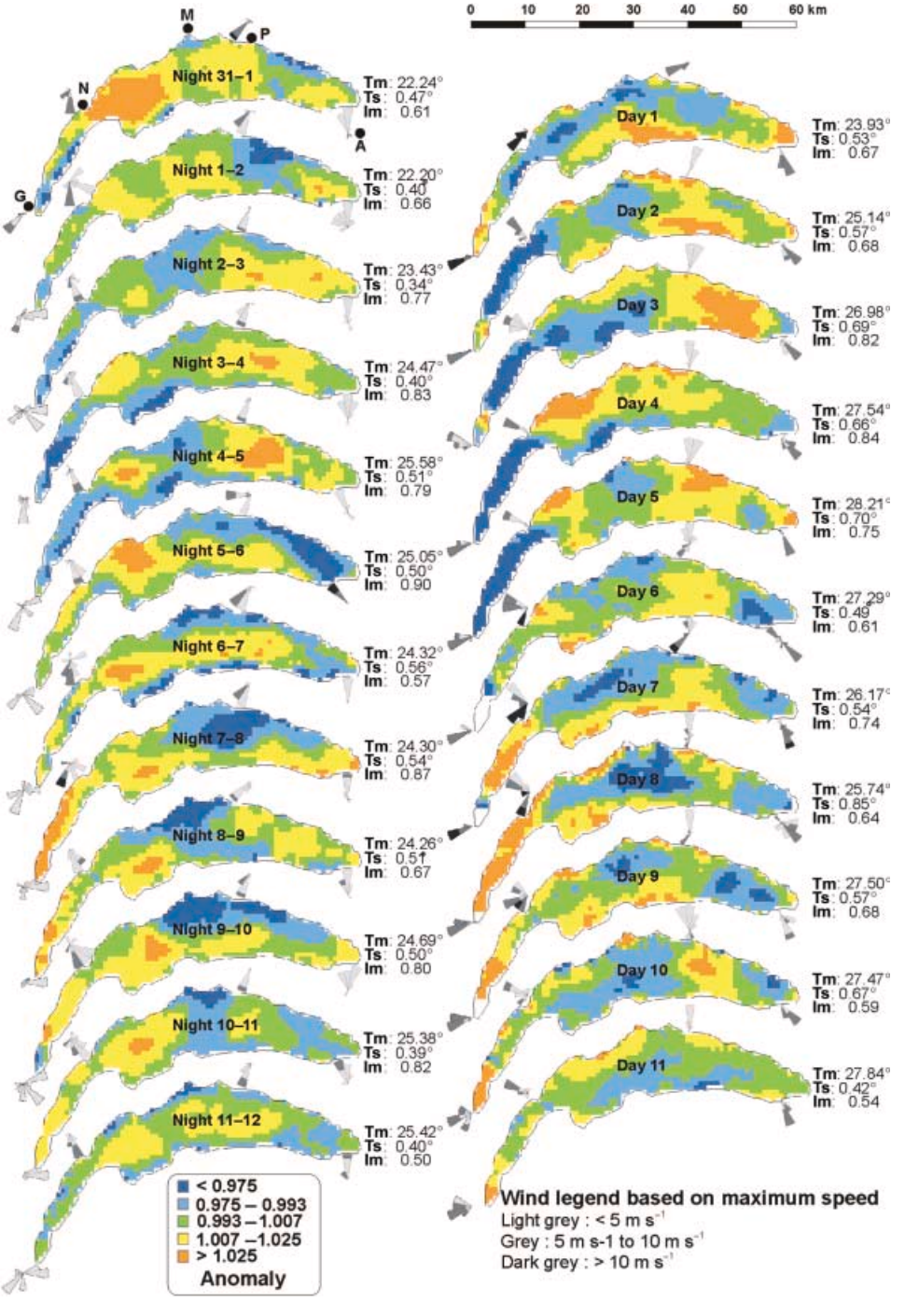

Figure 7. Diurnal and nocturnal LSWT climatology for Lake Geneva for the period from 31 July to 11 August 2003, expressed as anomaly maps (°C). Wind roses represent hourly wind direction and maximum wind speed at Geneva airport, Changins, Pully and Aigle meteorological stations. Lakewide statistics shown are Tm^n (lakewide nocturnal average), Tm^d (lakewide diurnal average), Ts^n (lakewide nocturnal standard deviation), Ts^d (lakewide diurnal standard deviation) and Im (Moran's first lag autocorrelation coefficient). G: Geneva; N: Nyon-Changins; M: Morges; P: Pully; A: Aigle.

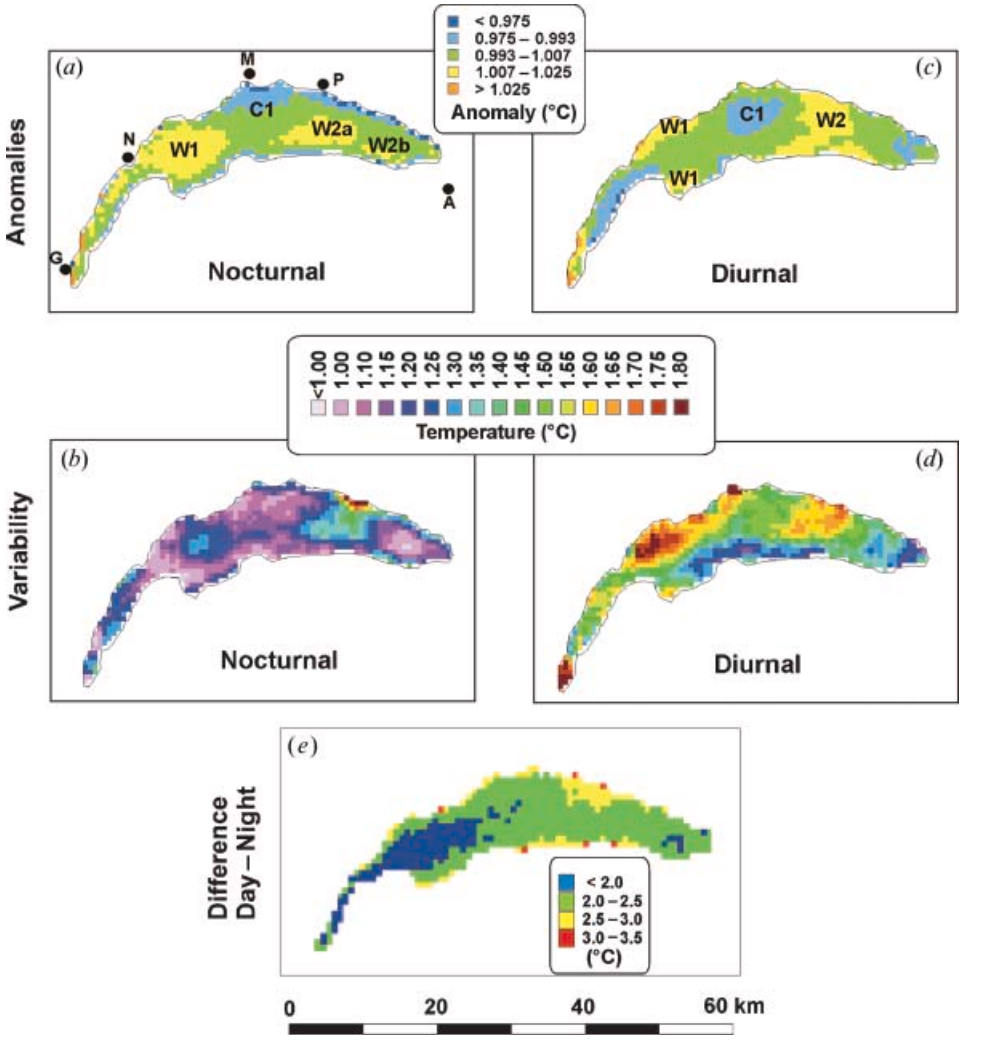

Figure 8. Quasi-decadal LSWT anomaly maps of Lake Geneva for 31 July to 11 August 2003. (*a*)Nocturnal and (*c*) diurnal, with the position of the eastern (W1) and western (W2, W2a, W2b) warm cores and the cold central ridge (C1). (*b*) and (*d*) Quasi-decadal LSWT variability maps, respectively. (*e*) Map of quasi-decadal LSWT difference between day and night ([ΔT_{d-n}]). To correct for diurnal thermocline effect, subtract 0.7°C. G: Geneva; N: Nyon-Changins; M: Morges; P: Pully; A: Aigle.

average, slightly higher at night (0.73) than during the day (0.69), indicating that patterns are more developed and coherent in night images. The lowest Moran autocorrelation coefficient values (close to 0.50; night 11–12) seem to be due to the presence of very small, cold anomalies occurring in coastal waters and possibly of an artificial nature (residual land contamination).

Night and day patterns are different in terms of anomalies: there is a greater likeness between the successions of night images than from one night image to that of the same day (e.g. nights 31–1 and night 1–2 versus night 31–1 and day 1 in figure 7). Day patterns do inherit some of the features of the preceding night (night

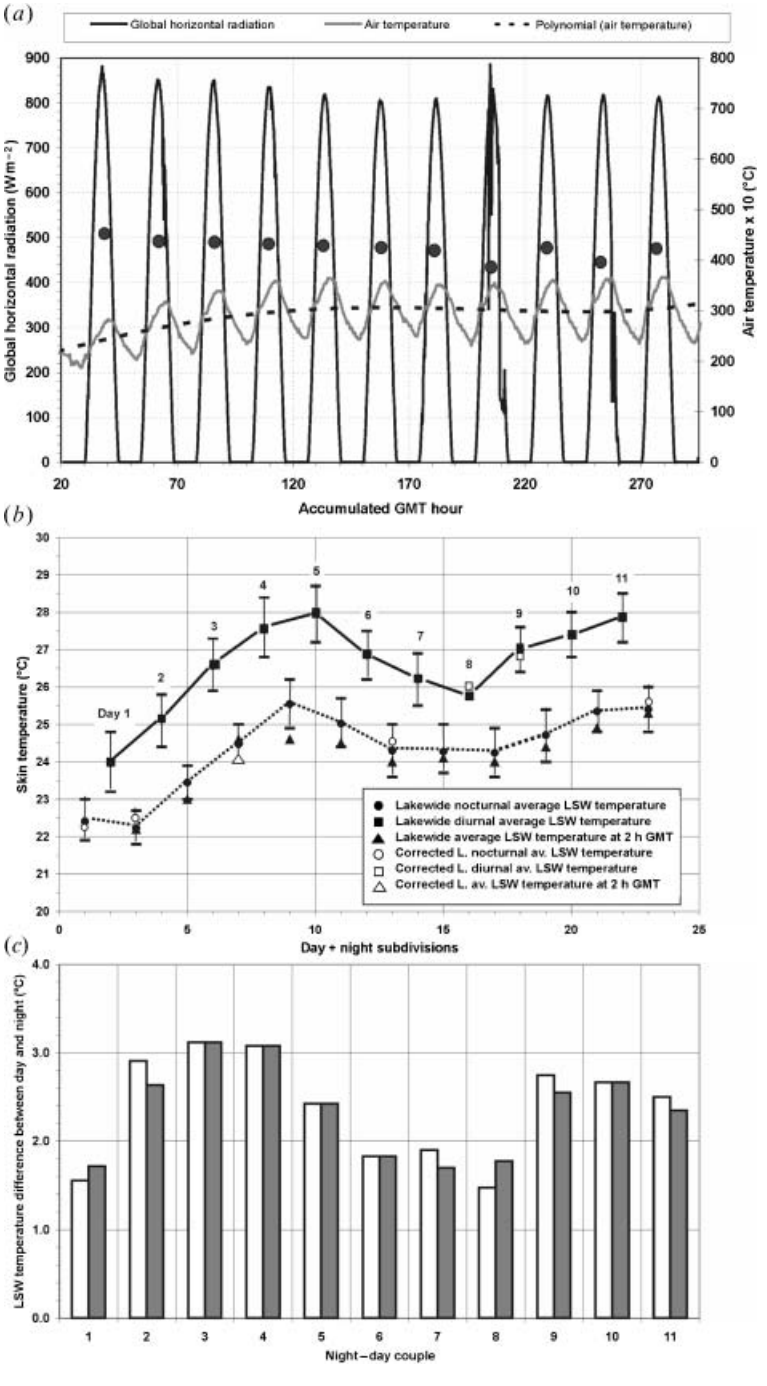

Figure 9. (*a*) Evolution of global horizontal radiation (daily averages as dots) and air temperature in Geneva, with fourth-degree polynomial trend. Start: night 31 July, hour 20. End: night 11 to 12 August. (*b*) Evolution of lakewide nocturnal and diurnal LSWT (black symbols), with ± 1 standard deviation intervals. Empty symbols are corrected temperature values. (*c*) Evolution of LSW thermal contrast $\Delta T_{\mathrm{d-n}}$. Mean value for period is $+2.3^{\circ}$C. White columns are raw data and grey columns are corrected as per figure 9(*b*). For diurnal thermocline correction, subtract 0.7°C from corrected values.

4–5 and day 5 for example), especially in the Petit Lac, but show either weakening (day 5) or inversion of anomalies (day 1; at the entrance to the Petit Lac).

The degree of permanence for night and day patterns is illustrated by the climatologies computed over the quasi-decadal period (11 days). For night situations (left column of figure 7 and figure 8(*a*)), two main warm cores permanently exist at the western (W1) and eastern ends (W2) of the Grand Lac, the eastern one being subdivided into two parts (W2a, W2b). These main warm cores are separated by a saddle-shaped cold anomaly (C1), which seems to be the most permanent feature in the lake (lowest standard deviation in figure 8(*b*)). There is no clear, predominant thermal pattern in Petit Lac during the night. In daytime (figure 8(*c*)), cold/warm cores are somewhat disturbed: C1 is disconnected from the north shore, whereas the opposite happens with W1 and W2. In the Petit Lac, however, a cold to warm gradient exists from the NE to the SW.

The extent of differences between day and night patterns is shown by the map of quasi-decadal LSWT difference ($[\Delta T_{d-n}]=[gmTS_d] - [gmTS_n]$) (figure 8(*e*)). Again, patterns are coherent and non-random (Moran Im=0.71). Petit Lac and the domain of warm core W1 show little thermal contrast (<2°C), in opposition to the coastal zone of Grand Lac (up to 3°C). There are also small differences in the Haut Lac, downstream from the Rhône valley.

3.7 *Time evolution of lakewide LSWT average*

The chronological evolutions of Tm_i (instantaneous averages) and Tm^n and Tm^d (diurnal and nocturnal averages) for the whole period are given in figures 6 and 9, respectively. They are characterized by the nycthemeral cooling–warming cycle of the lake surface, superimposed on a broader trend of heat accumulation between 31 July and 5 August, followed by a slight decrease before a moderate growth from 9 August in (figure 9(*b*)). The low Tm^d on 8 August (figure 6) corresponds essentially to a decreased radiation input due to partial cloud cover (figure 9(*a*)), and very little to the fact that the only instantaneous LSWT map available is at 0946 UTC, which is early in the morning (raw and corrected values are very close; table 2, line day 08.08).

As shown in figure 6, the Tm^d reaches a maximum between 12 and 15 UTC (i.e. 14–17 h in local summer time), about 1 h earlier than the air (top panel of figure 9) and roughly at the same time as the maximum radiation. At night, the minimum LSWT is reached between 2 and 6 UTC (4–8 h). These figures are similar to those reported for Lake Constance by Schneider and Mauser (1991). The time evolution of thermal amplitude between day and night ($\Delta T_{d-n}=Tm^d - Tm^n$) is shown in figure 9 (bottom panel).

4. Discussion

4.1 *Availability of thermal AVHRR imagery*

Taking the available AVHRR data for 2003 as a representative sample, our results show that satellite-based LSWT products have an adequate temporal resolution to observe, in Lake Geneva, both day and night LSWT patterns up to diurnal resolution. Limitations are due to periods of persistent cloud coverage resulting in only partial information for up to 20 days. Generally, at least one data set within a month covers more than 80% of the lake. The coverage could be increased in the future with the establishment of a cloud radiation and current-based lake surface

temperature model for interpolation, as suggested by Jin (2000) and Schwab *et al.* (1999). During cloud-free conditions, as illustrated for a selected period of 13 days in July to August, the LSWT maps allow the monitoring of the interdiurnal development of the surface thermal pattern (figures 5 and 7).

The main problems using an automated procedure for the computation of LSWT maps are, on one hand, scattered, missing pixels due to the cloud masking scheme (cases 5 and 6 in figure 4) and, on the other hand, land-contaminated, nearshore pixels produced by geometrical resampling (case 10 in figure 4). Both these issues have to be taken into account before further application of the data. Overall, the availability of information on the spatial temperature distribution, compared to the relatively scanty in situ data set, offers new insight into physical processes involved at the lake surface.

The patterns observed on AVHRR- and MODIS-based LSWT maps could be confirmed by high resolution Landsat TM temperature index (map 8 in figure 5). This type of data compensates the disadvantage of a low time frequency (less than 5 usable images per year in Switzerland) by a spatial resolution of 60 m. Whenever available, TM thermal data provide a 'zooming' tool on the coarser patterns derived from AVHRR or MODIS (Schneider *et al.* 1990).

4.2 *Depth representativity of LSWT patterns*

Both the daily and quasi-decadal LSWT patterns mapped from the AVHRR and MODIS images have been shown to be non-random and coherent. In order to use these maps towards an understanding of Lake Geneva physical limnology, we have first to ascertain that these patterns portray not only surface conditions, but are also similar to, or indicators of, thermal structures existing in deeper water layers (of the order of metres or tens of metres).

A useful frame of reference is provided by the idealised near-surface water temperature profiles of Donlon *et al.* (2002) and by the empirical model of the diurnal cycle of ΔSST of Gentemann *et al.* (2003), for the difference between skin temperature (Tskin) and bulk temperature at a depth of x metres (Tbulkxm), with x usually being between 1 and 5 m. Taking the night duration selected in the present study (20–8 h GMT), we have run the model of Gentemann *et al.* (2003) for AVHRR data, with a top-of-atmosphere mean solar insolation of $435\,\mathrm{Wm}^{-2}$ (representative of Lake Geneva conditions in August 2003) and a wind speed of $0\,\mathrm{ms}^{-1}$ (this last value was chosen because it yields the largest ΔSST). In this, the temperature difference goes from $+0.2^{\circ}\mathrm{C}$ at 20 h to a negative maximum of $-0.18^{\circ}\mathrm{C}$ at 7 h UTC and $0^{\circ}\mathrm{C}$ at 8 h, giving an average $\Delta\mathrm{SST} = +0.03^{\circ}\mathrm{C}$. From these results, and also from the similarity between the successive nocturnal anomalies of figure 7, we can consider that (a) AVHRR- and MODIS-derived nocturnal LSWT is representative of the lake bulk (epilimnetic) temperature and (b) LSWT patterns are a valid proxy for epilimnetic patterns.

The development of a so-called diurnal thermocline (Donlon *et al.* 2002, Minnett 2003, Oesch *et al.* 2005) leads to what has been termed decoupling of the LSWT from the bulk temperatures. Re-applying the model of Gentemann *et al.* (2003) to our diurnal conditions (8–20 h), again for a wind speed of $0\,\mathrm{ms}^{-1}$ (worst case), we found an average $\Delta\mathrm{SST} = +0.70^{\circ}\mathrm{C}$. Given this overall diurnal warming, there are two reasons to accept a decoupling of skin and bulk temperature and hence, a dissimilarity of their patterns. The first one is that, as previously mentioned, the differences between successive diurnal and nocturnal anomalies are larger than

between successive nocturnal patterns that are considered representative of deeper structures. The second reason is that diurnal anomalies (right panel of figure 7) follow each other without visible coherence, as witnessed by a higher variability over the whole period (figure 8(*d*)).

4.3 *Thermal pattern forcing*

The quasi-decadal anomaly maps of figure 8 (top panels) clearly portray the contrast in predominant thermal patterns between night and day. As a matter of fact, an opposition of day and night patterns can be observed because of wind periodicity and insolation (figure 9); apart from two weak bise episodes that have no incidence on climatology, the wind regime is characterized by lake (day) and land (night) breezes blowing in opposite directions (wind roses in figure 7). However, night breezes from the land, generally funnelled by valleys, are stronger and less variable in direction. They strongly condition the nocturnal patterns, broadly characterised by offshore warmer cores (figure 8(*a*)) surrounded by colder inshore rims. In daytime, the diurnal thermocline built up by solar insolation warms up the uppermost water layer, which is then pushed towards the coasts by transient lake breezes, temporarily masking the night patterns.

The two warm cores W1 and W2 in the Grand Lac separated by a saddle-shaped cold anomaly (C1) can be assumed to be existent over time, as can be concluded from the lakewide climatological statistical parameters (figure 8(*b*)); the standard deviation map indicates that the most persistent feature is C1 (low variability), and that the rim of W1 is more stable than its centre, which moves within the western basin of the Grand Lac. High standard deviation values indicate transient features, such as the cold night plumes near Pully (figure 8(*b*)) or the bise-induced ones between Morges and Nyon (figure 8(*d*)).

These predominant nocturnal patterns can be matched to the summer circulation features established by Lemmin and D'Adamo (1996) and Lemmin (1998). Figure 10 summarises these findings. In summer, wind forcing on the lake is applied mostly through land and lake breezes. Land breezes issuing from the northern shore change direction from W to E, causing a curl of the wind field and applying a major and persistent forcing on the lake surface (symbolised by a block arrow on figure 10). This induces a SW to S current across the lake coinciding with C1, and representing the western section of a large, elliptic anticlockwise (cyclonic) gyre affecting the Haut Lac and marked by the warm W2 anomalies. From the continuity law, a clockwise or anticyclonic gyre is postulated by Lemmin (1998) in the western part of the Grand Lac, the existence of which is supported by the presence of W1. This current pattern was tested using the criteria of Strub and Powell (1986) and was found to represent direct circulation.

In spite of their relatively short duration (1–2 days), the direct effect of long-fetch winds are visible on diurnal and nocturnal climatology maps (figure 7). The weak bise episodes of days 1 and 7 induce cold anomalies at the western end of Grand Lac and warm ones, downwind, in the Petit Lac. They can be interpreted, respectively, as upwelling and downwelling, somewhat referable to the 4 July 1989 situation shown by Lemmin and D'Adamo (1996; figure 9), and similar to the partial upwellings reported in Lake Tahoe by Strub and Powell (1987) and Steissberg *et al.* (2005). Another forcing of interest, concerning the central eastern part of Grand Lac, is given by vaudaire episodes, a stormy wind blowing down the Rhône valley. The wind records at Aigle and Pully stations for night 5–6 and day 6 (figure 7) clearly show the stress

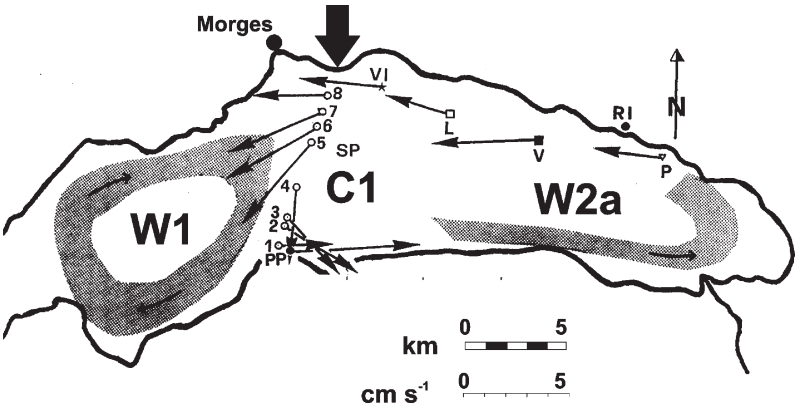

Figure 10. Summer large-scale circulation in Lake Geneva, from Lemmin (1998) with additions. Arrows with point symbol are mean current velocity in cm s^{-1} (0–20 m depth); grey strips are inferred current in cyclonic and anticyclonic gyres; black block arrows is the nocturnal land breeze (locally called a *morget*); W1, W2 are warm nocturnal anomalies; and C1 is the cold nocturnal anomaly.

exerted on the lake surface, giving rise to a large cold plume in the Haut Lac, followed by a smaller one west of Pully. They are visible on night and day images.

A strong increase in the Rhône river discharge is documented on days 5 and 6 (Anonymous 2004, p. 260), coinciding with the vaudaire rainstorm episode. A small cold plume at the Rhône river mouth was observed on some individual images, thus contributing to the cold anomaly visible on days 5 and 6 (figure 7). Such a phenomenon had already been observed by Giovanoli (1990).

4.4 *Diurnal warming–cooling cycle*

During the study period, the thermal evolution of the Lake Geneva surface layer is summarised by the lakewide LSWT day and night averages (figure 9(*b*)), and can be compared to the radiation and air temperature (figure 9(*a*)). Diurnal and nocturnal trends are roughly parallel. Surface temperature builds up until 5 August, then the trend is suddenly inverted for 3 days. No variation of the same kind is visible either in insolation until 8 August, or in air temperature, which merely stabilises. The reason for this heat loss (diurnal as well as nocturnal) is ascribed to the occurrence of two episodes of long-fetch wind mentioned above: the strong and sudden storm-generated vaudaire down the Rhône valley in the night of 5–6 August, and the NE bise episode of 6–8 August. After the re-installment of the breeze regime, heat accumulation resumes for the 3 last days (9–11 August).

Despite the time-series brevity, the evolution of difference within successive day–night couples (ΔT_{d-n}; figure 9(*c*)) is interesting. In the warming-up phase, ΔT_{d-n} builds up and reaches a maximum of 3°C (or more exactly, 2.3°C after deduction of the diurnal thermocline effect). It stabilises even though the LSWT continues rising, and then reaches a minimum during the synoptic wind mixing of the surface layer. This trait is confirmed by the patterns visible on the map of $[\Delta T_{d-n}]$ (figure 8(*e*)); minimal differences between day and night LSWT exist in the areas exposed to the influence of bise (western Grand Lac and Petit Lac) and vaudaire (Haut Lac), which occasionally attenuate or even destroy the diurnal thermocline through mixing.

5. Conclusions

For the Lake Geneva region, day and night coverage by AVHRR for the representative year 2003 is sufficient for at least weekly to monthly temporal resolution. Therefore, historical AVHRR data is suitable to exploit LSWT patterns of the last two decades. The concurrent coverage of AVHRR and MODIS sensors allows interdiurnal surface pattern studies. Future implementation of Meteosat 8 data with a temporal resolution of 15 min seems therefore to be promising for lake physics studies.

Errors related to viewing geometry and atmospheric effects were taken into account and could therefore be separated from effects related to the different depths of the water body.

The various day and night surface thermal patterns, observed by satellite imagery, could be linked to the thermal structure existing in the deeper water layers using the concept of the diurnal decoupling layer (Donlon *et al.* 2002, Minnett 2003, Oesch *et al.* 2005) and the empirical model of the diurnal cycle of ΔSST of Gentemann *et al.* (2003).

The daily thermal pattern forcing could be explained by thermal breezes and insolation conditions. This induces a stable, south-trending cold surface jet across the central part of Grand Lac. During daytime, under the influence of insolation, a diurnal thermocline is built up and a warm topmost layer is pushed towards the shore by the transient lake breezes, temporarily erasing the night patterns. The persistent two warm cores and the saddle-shaped cold anomaly could be matched with the summer time circulation features established by Lemmin and D'Adamo (1996) and Lemmin (1998). From the continuity law, an anticyclonic gyre is postulated by Lemmin (1998) in the western part of Grand Lac, the existence of which is supported by the presence of a warm core (W1). The phenomenon of upwelling and downwelling in some regions is a direct effect of long-fetch winds during day and night situations. Another similar forcing-related phenomenon explains the large cold plume in the Haut Lac, introduced by the strong wind (vaudaire) blowing down the Rhône Valley.

The lakewide average LSWTs for day and night during the study period are roughly parallel. A sudden loss of stored heat, manifested by a sudden LSWT decrease could be explained by two episodes of long fetch NE wind (bise) that interrupted the breeze regime during 2 days.

Using space-borne medium resolution radiometers, operational monitoring of Lake Geneva LSWT is feasible. The LSWT information could potentially be assimilated for numerical lake modelling and hence be of significant interest for environmental and climatological research.

Acknowledgements

In situ temperature measurements were kindly provided by CIPEL (Lausanne) and meteorological data was provided by CUEPE (University of Geneva). We gratefully acknowledge the inspiration gained from the work of U. Lemmin (EPFL, Lausanne) on the physical limnology of Lake Geneva. The early versions of the manuscript were greatly improved thanks to the critical reading of two anonymous reviewers. We also thank the Editor for the final editing of our text.

References

Barsi, J.A., Schott, J.R., Palluconi, D.L., Hook, S.J., Markham, B.L., Chander, G. and O'Donnel, E.M., 2003, Landsat TM and ETM+ thermal band calibration. *Canadian Journal of Remote Sensing*, **29**, pp. 141–153.

BELETSKY, D. and SCHWAB, D.J., 2001, Modeling circulation and thermal structure in Lake Michigan: annual cycle and interannual variability. *Journal of Geophysical Research*, **106**, pp. 19 745–19 771.

BOHLE-CARBONELL, M., 1991, Wind and currents: response patterns of Lake Geneva. *Annales Geophysicae. Atmospheres, Hydrospheres and Space Sciences*, **9**, pp. 82–90.

BOUET, M., 1985, *Climat et Météorologie de la Suisse Romande* (Lausanne: Payot).

BUSSIÈRES, N., VERSEGHY, D. and MACPHERSON, J.I., 2001, The evolution of AVHRR-derived water temperatures over boreal lakes. *Remote Sensing of Environment*, **80**, pp. 373–384.

CIPEL, 2005, *Rapport sur les études et recherches entreprises dans le bassin lémanique. Campaign 2004.* Available online at: http://www.cipel.org/sp/IMG/pdf/rap-2004.pdf.

COX, C. and MUNK, W., 1954, Measurement of the roughness of the sea surface from photographs of the Sun's glitter. *Journal of the Optical Society of America*, **44**, pp. 838–850.

DONLON, C.J., MINNETT, P.J., GENTEMANN, C., NIGHTINGALE, T.J., BARTON, I.J., WARD, B. and MURRAY, M.J., 2002, Toward improved validation of satellite sea surface skin temperature measurements for climate research. *Journal of Climate*, **15**, pp. 353–369.

FAOUR, G., SHABAN, A. and JAQUET, J.M., 2004, Contribution of the thermal infrared band of Landsat-7 ETM+ in the detection of seawater pollution along the Lebanese shoreline. *Télédétection*, **4**, pp. 197–209.

GENTEMANN, C.L., DONLON, C.J., STUART-MENTETH, A. and WENTZ, F.J., 2003, Diurnal signals in satellite sea surface temperature measurements. *Geophysical Research Letters*, **30**, pp. 40-1–40-4.

GIOVANOLI, F., 1990, Horizontal transport and sedimentation by interflows and turbidity currents in Lake Geneva. In *Large Lakes: Ecological Structure and Function*, M.M. Tilzer and C. Serruya (Eds), pp. 176–195 (Springer).

GOODCHILD, M.F., 1988, Spatial autocorrelation. In *Concepts and Techniques in Modern Geography*, (CATMOG) Number **47** (Norwich: Geobooks).

GOODRUM, G., KIDWELL, K.B. and WINSTON, W., 2000, *NOAA KLM user's guide.* U.S. Department of Commerce, National Oceanic and Atmospheric Administration, National Environment Satellite, Data and Information Service, National Climatic Data Center, Climate Services Division, Satellite Services Branch, Suitland, MD, USA. Available online at: http://www2.ncdc.noaa.gov/docs/klm/cover.htm.

IMBERGER, J. and PATTERSON, J.C., 1990, Physical limnology. *Advances in Applied Mechanics*, **27**, pp. 303–475.

JIN, M., 2000, Interpolation of surface radiative temperature measured from polar orbiting satellites to a diurnal cycle 2. Cloudy-pixel treatment. *Journal of Geophysical Research*, **105**, pp. 4061–4076.

KEY, J.R., 2002, The cloud and surface parameter retrieval (CASPR) system for polar AVHRR, Cooperative Institute for Meteorological Satellite Studies, University of Wisconsin, Madison. Available online at: http://stratus.ssec.wisc.edu/caspr/.

LANDESHYDROLOGIE (Ed.), 2004, Annuaire hydrologique de la Suisse, year 2003. Available online at: http://www.bafu.admin.ch/php/modules/shop/files/pdf/phpHZmDhg.pdf.

LANE, R.K., 1970, Great Lakes thermal studies using infrared imagery. *Limnology and Oceanography*, **15**, pp. 296–300.

LEMMIN, U., 1998, Courantologie lémanique. *Archives des Sciences, Geneva*, **51**, pp. 103–120.

LEMMIN, U. and D'ADAMO, N., 1996, Summertime winds and direct cyclonic circulation: observations from Lake Geneva. *Annales Geophysicae*, **14**, pp. 1207–1220.

LEMMIN, U., MORTIMER, C.H. and BÄUERLE, E., 2005, Internal seiche dynamics in Lake Geneva. *Limnology and Oceanography*, **50**, pp. 207–216.

LI, X., PICHEL, W., CLEMENTE-COLÓN, P., KRASNOPOLSKY, V. and SAPPER, J., 2001, Validation of coastal sea and lake surface temperature measurements derived from NOAA/AVHRR data. *International Journal of Remote Sensing*, **22**, pp. 1285–1303.

MINNETT, P.J., 2003, Radiometric measurements of the sea-surface skin temperature: the competing roles of the diurnal thermocline and the cool skin. *International Journal of Remote Sensing*, **24**, pp. 5033–5047.

MINNETT, P.J., EVANS, R.H., KEARNS, E.J. and BROWN, O.B., 2002, Sea-surface temperature measured by the moderate resolution imaging spectroradiometer (MODIS). In *Proceedings of IEEE International Geoscience and Remote Sensing Symposium, IGARSS 2002*, **2**, 24–28 June 2002, Toronto, Ontario, Canada.

MONISMITH, S.G., 1985, Wind-forces motion in stratified lakes and their effect on mixed layer shear. *Limnology and Oceanography*, **30**, pp. 771–783.

MONISMITH, S.G., 1986, An experimental study of the upwelling response of stratified reservoirs to surface shear stress. *Journal of Fluid Mechanics*, **171**, pp. 407–439.

MORTIMER, C.H., 1952, Water movements in lakes during summer stratification: Evidence from distribution of temperature in Windmere. *Philosophical Transactions of Royal Society*, **B236**, pp. 355–404.

NOBLE, V.E. and WILKERSON, J.C., 1970, Airborne temperature surveys of Lake Michigan: October 1966 to October 1967. *Limnology and Oceanography*, **15**, pp. 289–296.

NOTARSTEFANO, G., MAURI, E. and POULAIN, P.-M., 2006, Near-surface thermal structure and surface diurnal warming in the Adriatic Sea using satellite and drifter data. *Remote Sensing of Environment*, **101**, pp. 194–211.

OESCH, D., JAQUET, J.-M., HAUSER, A. and WUNDERLE, S., 2005, Lake surface water temperature retrieval using AVHRR and MODIS data: validation and feasibility study. *Journal of Geophysical Research*, **110**, pp. C12014.

SCHNEIDER, K. and MAUSER, W., 1991, The impact of the meteorological situation upon the satellite-derived surface skin temperature. In *Proceedings of 11*th *EARSeL Symposium*, Graz, Austria, pp. 270–285.

SCHNEIDER, K., MAUSER, W. and GRUNWALD, B., 1990, The detrmination of energy fluxes at the water surface of Lake Constance using remotely sensed data. *Verhandlungen der Internationalen Vereinigung für Limnologie*, **24**, pp. 73–79.

SCHWAB, D.J. and BELETSKY, D., 2003, Relative effects of wind stress curl, topography, and stratification on large-scale circulation in Lake Michigan. *Journal of Geophysical Research*, **108**, pp. C23044.

SCHWAB, D.J., LESHKEVICH, G.A. and MUHR, G.C., 1992, Satellite measurements of surface water temperature in the great lakes: Great Lakes coastwatch. *Journal of Great Lakes Research*, **18**, pp. 247–258.

SCHWAB, D.J., LESHKEVICH, G.A. and MUHR, G.C., 1999, Automated mapping of surface water temperature in the Great Lakes. *Journal of Great Lakes Research*, **25**, pp. 468–481.

STEISSBERG, T.E., HOOK, S.J. and SCHLADOW, S.G., 2005, Characterizing partial upwellings and surface circulation at Lake Tahoe, California, Nevada, USA with thermal infrared images. *Remote Sensing of Environment*, **99**, pp. 2–15.

STRUB, P.T. and POWELL, T.M., 1986, Wind-driven surface transport in stratified closed basins: direct versus residual circulations. *Journal of Geophysical Research*, **91**, pp. 8497–8508.

STRUB, P.T. and POWELL, T.M., 1987, Surface temperature and transport in Lake Tahoe: inferences from satellite (AVHRR) imagery. *Continental Shelf Research*, **7**, pp. 1001–1013.

THIEMANN, S. and SCHILLER, H., 2003, Determination of the bulk temperature from NOAA/AVHRR satellite data in a midlatitude lake. *International Journal of Applied Earth Observation and Geoinformation*, **4**, pp. 339–349.

WALTON, C.C., PICHEL, W.G., SAPPER, J.F. and MAY, D.A., 1998, The development and operational application of nonlinear algorithms for the measurement of sea surface temperatures with the NOAA polar-orbiting environmental satellites. *Journal of Geophysical Research*, **103**, pp. 27 999–28 012.

WANNER, H. and FURGER, M., 1990, The Bise-climatology of a regional wind north of the Alps. *Meteorology and Atmospheric Physics*, **43**, pp. 105–115.

WESSEL, P. and SMITH-WALTER, H.F., 1996, *A global, Self-consistent, Hierarchical, High-resolution Shoreline Database* (Washington DC: American Geophysical Union).

WOOSTER, M., PATTERSON, G., LOFTIE, R. and SEAR, C., 2001, Derivation and validation of the seasonal thermal structure of Lake Malawi using multi-satellite AVHRR observations. *International Journal of Remote Sensing*, **22**, pp. 2953–2972.